NASA-CR-202712

N 2 B

The infrared spectrum of H_2S from 1 to 5 μm

ALEXANDER D. BYKOV, OLGA V. NAUMENKO, MAXIM A. SMIRNOV, AND LEONID N. SINITSA
Institute of Atmospheric Optics, SB, Russian Academy of Science, Tomsk, Russia

AND

LINDA R. BROWN,[1] JOY CRISP, AND DAVID CRISP
Jet Propulsion Laboratory, California Institute of Technology, Pasadena, CA 91109, U.S.A.

7N-32-CR

Received March 21, 1994
Accepted July 5, 1994

This paper is dedicated to Dr. Gerhard Herzberg on the occasion of his 90th birthday

The absorption spectra of H_2S from 2000 to 11 147 cm^{-1} have been obtained with spectral resolutions of 0.006, 0.012, and 0.021 cm^{-1} using the Fourier transform spectrometer at Kitt Peak National Observatory. The transitions of 21 bands have been assigned for the first time and 9 others reanalyzed so that accurate energy levels, band origins, and rotational parameters could be determined. The analysis of these data revealed some remarkable features in the energy spectrum, e.g., fourfold clustering of rotational levels belonging to the symmetric and asymmetric components of local mode manifolds at a high degree of stretching excitation. This paper reports fitted vibrational parameters and predicted band origins of $H_2{}^{32}S$ up to 12 735 cm^{-1}. It also presents the degenerate rotational constants and upper state energies of (301)–(202) and (311)–(212) at 1 μm as illustrations of clustering in the local mode limit.

Les spectres d'absorption de H_2S entre 2000 et 11 147 cm^{-1} ont été obtenus avec des résolutions spectrales de 0,006, 0,012 et 0,021 cm^{-1}, en utilisant le spectromètre à transformée de Fourier du Kitt Peak National Observatory. Les transitions de 21 bandes ont été identifiées pour la première fois, et 9 autres ont été réanalysées de façon à pouvoir déterminer avec précision les niveaux d'énergie, les origines de bandes et les paramètres rotationnels. L'analyse de ces données a révélé quelques particularités remarquables du spectre d'énergie, entre autres le groupement quadruple de niveaux rotationnels appartenant aux composantes symétriques et asymétriques d'ensembles de modes locaux à un haut degré d'excitation d'allongement. On donne dans cet article des valeurs ajustées des paramètres vibrationnels, ainsi que des prédictions pour les origines de bandes de $H_2{}^{32}S$ jusqu'à 12 735 cm^{-1}. On présente aussi les constantes rotationnelles dégénérées et les énergies des états supérieurs de (301)–(202) et (311)–(212) à 1 μm, comme illustration du groupement à la limite des modes locaux.

[Traduit par la rédaction]

Can. J. Phys. **72**, 989 (1994)

1. Introduction

The detailed knowledge of hydrogen sulfide absorption spectra has application for terrestrial atmospheric pollutant measurements and for the investigation of chemistry in the atmospheres of Venus and the outer planets. From a theoretical viewpoint, hydrogen sulfide is an interesting example of a light asymmetric rotor for which the internal nuclear motion can be strongly perturbed by intramolecular interactions arising from vibrational or rotational excitation. For this reason, the vibrational–rotational energy spectrum of H_2S has been modeled in numerous papers using new theoretical approaches to demonstrate the effects of the local mode vibrations or bending–rotation coupling [1–3]. The infrared spectrum of H_2S has been the subject of several high-resolution studies concerning the ground vibrational state [4, 5], the first excited level (010) at 8.3 μm [6, 7], the first triad of interacting states {(020)–(100)–(001)} at 4 μm [8], two levels {(110)–(011)} from the second triad at 2.7 μm [9], and the {(101)–(200)} [10] and {(111)–(210)} [11] states belonging to the first and second hexades at 2 μm and 1.6 μm, respectively. However, up to now, the knowledge of hydrogen sulfide absorption and its energy spectrum has been incomplete, especially in the case of weak overtone stretching and bending modes. The lack of experimental data has limited both the theoretical analysis and the prediction of the near-infrared and the visible regions.

The present study reports the vibrational assignment of $H_2{}^{32}S$ over a wide spectral interval from 2000 to 11 147 cm^{-1}. Figure 1 shows a composite spectrum obtained from two different optical densities. In all, transitions of a total of 30 vibrational bands have been observed. Of these, 21 bands, including (311) at 11 008 cm^{-1}, have been identified at high-resolution for the first time. In this report, we present the vibrational energy levels analysis along with the rotational assignments at 1 μm of pairs of parallel and perpendicular bands that become rotationally degenerate in the local mode limit.

2. Experimental details

Laboratory spectra of H_2S were recorded at 0.006, 0.012, and 0.020 cm^{-1} resolution with the Fourier transform spectrometer located at the McMath telescope facility at Kitt Peak National Observatory/National Solar Observatory. Data were obtained using three different beamsplitters (KCl, CaF_2, and quartz) in conjunction with As-doped silicon, InSb, and photo-diode detectors in five different band pass intervals: 1000–2600 cm^{-1}, 1800–5500 cm^{-1}, 3600–9000 cm^{-1}, 3600–13 000 cm^{-1}, and 8600–16 000 cm^{-1}. The optical sources were a globar at longer wavelengths and a quartz projection lamp in the near-infrared and visible regions. Optical path lengths were changed from 1.5 m to a maximum of 433 m by using three different stainless steel absorption cells. Sample pressures were varied from 1.49 to 30 Torr (1 Torr = 133.3 Pa) at room temperature. For some scans, a second absorption cell containing CO was placed in series with the H_2S cell to establish the frequency calibration in the near-infrared using the 2–0 positions reported by Pollock et al. [12]. Each spectrum was usually integrated 70–80 min to produce signal-to-noise ratios ranging from

[1]Author to whom correspondence may be addressed.

Printed in Canada / Imprimé au Canada

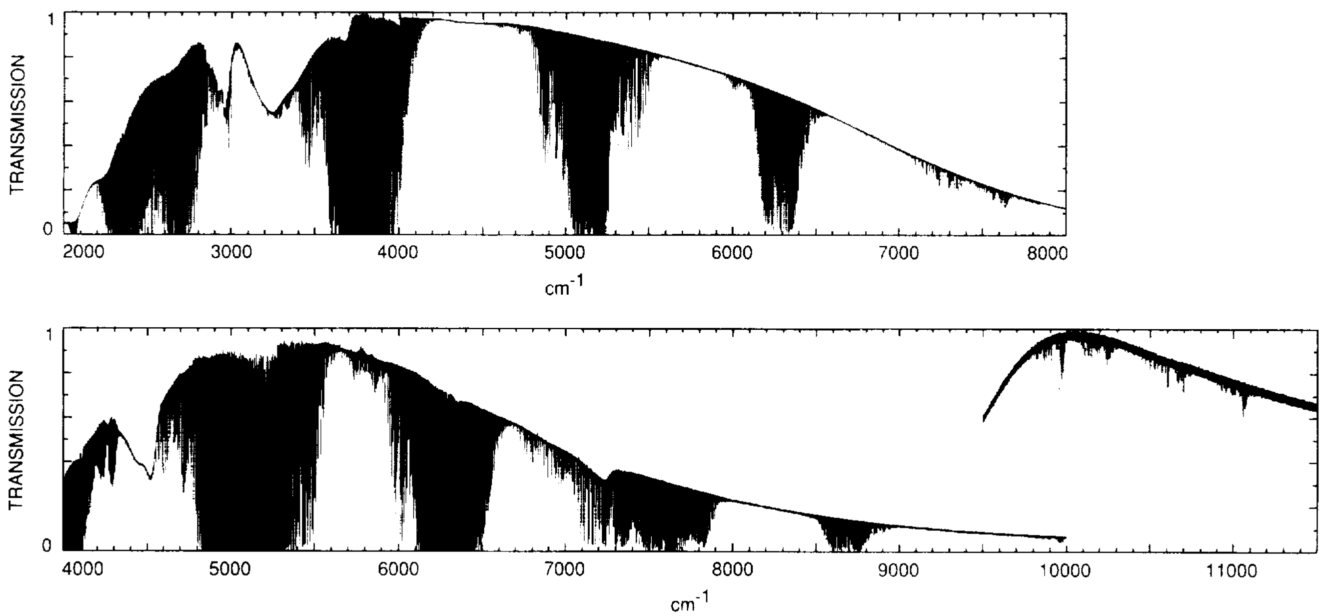

FIG. 1. The observed spectra of H_2S recorded at two optical densities. Top: 28.5 m with 9.99 Torr at 289 K. Bottom: 433 m with 29.9 Torr at 298 K. The upper panel shows the portions from the 1800–5500 and 3600–9000 cm^{-1} band passes, which are joined together at 4000 cm^{-1}. The lower frame is taken from the 3600–13 000 (left) and 8600–16 000 (right) cm^{-1} band passes. Spectral impurities arise from H_2O at 3700, 5300, 7200, 8890, and 1060 cm^{-1}; CO_2 at 2350 and 3714 cm^{-1}; SO_2 at 2100, C_2H_6 at 2980, and HCN at 3300 cm^{-1}.

TABLE 1. Summation of assigned levels for 27 H_2S bands in the near-infrared*

System	Region (μm)	Band	J_{max}	K_a (max)	Number
Second triad	2.7	030	8	6	41
		110	10	7	94
		011	10	7	100
First hexade	2.0	040	9	7	54
		120	10	7	73
		021	11	9	115
		200	11	10	124
		101	11	10	128
		002	11	6	68
Second hexade	1.6	050	12	5	65
		130	8	7	63
		031	8	7	65
		210	8	7	67
		111	8	7	60
First decade	1.3	121	7	6	65
		102	8	7	75
		201	8	8	74
		300	8	8	75
		003	8	8	76
Second decade	1.1	112	9	7	74
		211	9	8	86
First or second pentadecades	1	301	8	8	74
		202	8	7	47
		400	9	8	58
		103	9	8	67
		311	8	8	63
		212	7	7	35

*SYSTEM indicates the total number of interacting states: triad (3), hexade (6), decade (10), and pentadecade (15). BAND is the quanta of $\nu_1\nu_2\nu_3$ (110, 011, 101, 002, 210, and 111 have been previously studied at high resolution). NUMBER shows the total number of upper state levels assigned to maximum J and K_a.

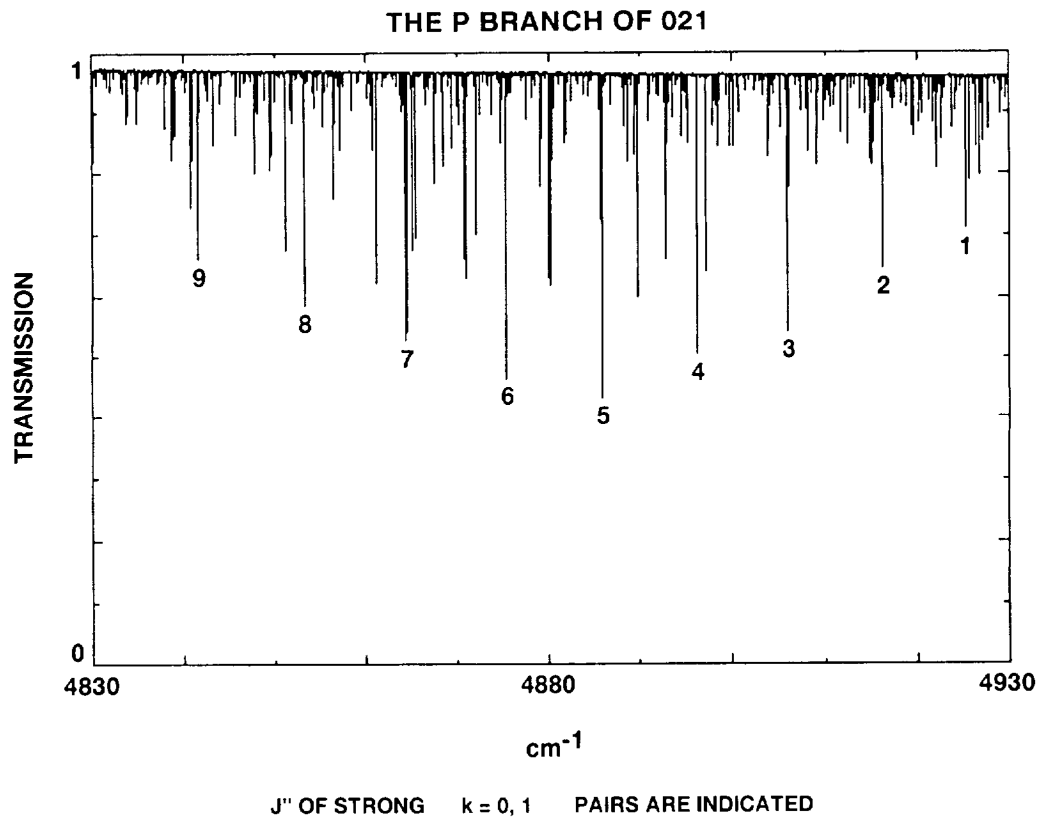

FIG. 2. An apodized Kitt Peak FTS spectrum of H_2S in the P-branch region of (021). The J'' assignments of the $K_a = 0,1$ lines are indicated. The optical path is 28.5 m, and the sample pressure is 9.99 Torr at 289 K.

1000:1 at 2.5 μm to 400:1 at 8 μm to 50:1 at 1 μm. Figure 1 gives a composite spectra obtained with the last four band passes: the top was recorded with a 28 m optical path and 9.99 Torr of H_2S at 289 K; the two band passes are joined together at 4000 cm^{-1}. The bottom trace was obtained with a 433 m path and 29.9 Torr at 298 K.

The line centers were determined either by doing first and second derivatives of the apodized spectra or by least-squares fitting of the Voigt contour with the unapodized data. The precision and accuracy of a line center varied according to the region, gas pressure, and degree of blending with other features. Between 2000 and 5500 cm^{-1}, where the resolution was 0.012 cm^{-1}, the precision is 0.0002 cm^{-1}, and the accuracy is 0.0004 cm^{-1} or better for strong, isolated lines. For weak lines and all lines above 6600 cm^{-1}, these values are worse by a factor of two because of the reduced signal-to-noise ratio. However, at 11 000 cm^{-1} where the resolution was 0.021 cm^{-1}, the precision at best is 0.0010 cm^{-1} because the signal-to-noise ratio was poor. In addition, higher sample pressures of 10–30 Torr were required to observe these very weak bands so that line centers were affected by pressure shifts. The absolute line positions were further degraded because no suitable calibration lines were available near 1 μm; for the interim, these data were calibrated using H_2S lines at 8800 cm^{-1} recorded using the 3600 to 13 000 cm^{-1} band pass with the same gas sample. Overall, the accuracy of the near-infrared positions between 8000 and 11 000 cm^{-1} is estimated to be 0.005 cm^{-1} or better.

3. Line assignments and rotational energy levels

The line assignments were made using the combination differences and estimated line frequencies and strengths as described in ref. 13. The line assignment process was followed by continual fitting of the rotational constants to obtain better predicted line positions and relative strengths. Such a procedure often permitted the identification of weak lines that could not be assigned by usual combination difference methods. Table 1 summarizes the upper vibrational states of 27 bands belonging to different interacting band systems (triad, hexade, decade, and pentadecade) that have been observed so far in the near-infrared portion of the Kitt Peak spectra. The extent of identification is given by indicating the largest values of the J and K_a quantum numbers (J_{max} and K_a(max)) obtained up to now and the total number of upper state levels assigned. Figure 2 shows the P branch of (021) recorded at 0.012 cm^{-1} resolution with a 28 m optical path and 9.99 Torr of H_2S at 289 K. Table 2 lists the observed band centers for 31 energy states; the value of the lowest fundamental is from ref. 7. All but five band origins were obtained using the observed assignment of $P(1,1,1)$ or $P(1,0,1)$ to the 0,0,0 levels. Table 2 also lists the experimental line positions and corresponding intensities (in cm^{-2} atm^{-1} at room temperature; 1 atm = 101.3 kPa) of the $P1$ lines. For the (040), (050), (202), (212), and (400) states, the band centers were determined by fitting available assignments because the $P1$ lines were too weak to be observed. The accuracy of these fitted values ranges from 0.002 to 0.005 cm^{-1}.

TABLE 2. Observed* and calculated vibrational upper state energy levels of $H_2{}^{32}S$

v_1	v_2	v_3	Local $nm+/-v$	E_{calc} (cm^{-1})	E_{obs} (cm^{-1})	(obsd. − calc.) ($cm^{-1} \times 10^{-3}$)	$P1\ \nu$ (cm^{-1})	$P1$ Int ($cm^{-2}/atm \times 10^{-5}$)	Kozin [3] MORBID	Senekowitsch [15] ab initio
0	1	0	00+1	1 182.561	1 182.5742	14	1 167.4851	145.	1 182.44	1 190.4
0	2	0	00+2	2 353.950	2 353.9644	14	2 338.8743	47.6	2 353.83	2 372.0
1	0	0	10+0	2 614.355	2 614.4080	53	2 599.3179	29.3	2 614.66	2 620.4
0	0	1	10−0	2 628.431	2 628.4551	24	2 614.7079	3.9	2 628.56	2 631.0
0	3	0	00+3	3 513.789	3 513.7900	1	3 498.6999	6.8	3 513.17	3 543.5
1	1	0	10+1	3 779.179	3 779.1665	−12	3 764.0764	282.	3 779.29	3 794.6
0	1	1	10−1	3 789.273	3 789.2688	−4	3 775.5226	980.	3 789.66	3 799.8
0	4	0	00+4	4 661.699	‡4 661.6770	−22	4 646.586	0.2	4 659.48	4 703.7
1	2	0	10+2	4 932.715	4 932.6992	−16	4 917.6091	1.8	4 932.91	4 960.1
0	2	1	10−2	4 939.122	4 939.1044	−17	4 925.3581	26.0	4 939.82	4 960.0
2	0	0	20+0	5 145.014	5 144.9862	−28	5 129.8961	45.3	5 145.52	5 154.2
1	0	1	20−0	5 147.256	5 147.2205	−36	5 133.4742	211.	5 147.12	5 155.5
0	0	2	11+0	5 243.055	5 243.1014	46	5 228.0113	9.6	5 243.38	5 251.2
0	5	0	00+5	5 797.300	‡5 797.235	−65	5 782.144	<.1	5 791.83	5 851.6
1	3	0	10+3	6 074.585	6 074.5823	−3	6 059.4922	0.6	6 074.50	6 115.6
0	3	1	10−3	6 077.597	6 077.5954	−2	6 063.8491	0.9	6 078.05	6 110.2
2	1	0	20+1	6 288.160	6 288.1462	−13	6 273.0561	9.4	6 288.37	6 307.7
1	1	1	20−1	6 289.220	6 289.1735	−47	6 275.4272	119.	6 288.99	6 307.8
0	1	2	11+1	6 386.119					6 385.89	6 403.0
0	6	0	00+6	6 920.212					6 909.29	6 986.4
0	4	1	10−4	7 204.320					7 203.39	7 249.4
1	4	0	10+4	7 204.410					7 203.10	7 259.8
2	2	0	20+2	7 419.818					7 420.03	7 451.5†
1	2	1	20−2	7 420.074	7 420.0923	17	7 406.3460	1.9	7 419.92	7 452.1
0	2	2	11+2	7 518.451					7 517.74	7 546.9†
1	0	2	30+0	7 576.395	7 576.3816	−14	7 561.2915	14.4	7 576.45†	7 589.4
2	0	1	30−0	7 576.555	7 576.5450	−11	7 562.7987	10.9	7 576.42	7 589.4
3	0	0	21+0	7 752.288	7 752.2644	−23	7 737.1743	1.1	7 752.40†	7 768.4
0	0	3	21−0	7 779.341	7 779.3195	−22	7 765.5732	2.2	7 779.60	7 789.3
0	7	0	00+7	8 030.058					8 010.95	8 307.0
0	5	1	10−5	8 318.912					8 314.90	8 376.5
1	5	0	10+5	8 321.811					8 317.74	8 391.7
1	3	1	20−3	8 539.438					8 538.93	8 585.9
2	3	0	20+3	8 539.684					8 539.53	8 585.3†
0	3	2	11+3	8 639.598					8 637.92	8 681.5†
1	1	2	30+1	8 697.070	8 697.142	72	8 682.052	0.4	8 696.58†	8 723.0
2	1	1	30−1	8 697.115	8 697.155	40	8 683.409	4.1	8 696.48	8 723.1
3	1	0	21+1	8 880.066					8 877.73†	8 906.9
0	1	3	21−1	8 899.270					8 898.66	8 917.4
0	8	0	00+8	9 126.455					9 095.86	
0	6	1	10−6	9 420.992					9 411.66	9 212.7
1	6	0	10+6	9 426.404					9 417.50	9 490.6
1	4	1	20−4	9 646.934					9 645.06	9 707.9

TABLE 2. (*concluded*)

v_1	v_2	v_3	Local $nm+/-v$	E_{calc} (cm^{-1})	E_{obs} (cm^{-1})	(obsd. − calc.) ($cm^{-1}\times10^{-3}$)	$P1\ \nu$ (cm^{-1})	$P1$ Int ($cm^{-2}/atm\times10^{-5}$)	Kozin [3] MORBID	Senekowitsch [15] ab initio
2	4	0	20+4	9 647.447					9 645.95	9 708.0
0	4	2	11+4	9 749.111					9 745.45	
2	2	1	30−2	9 806.479					9 805.37	9 805.6
1	2	2	30+2	9 806.482					9 805.50‡	9 847.8
2	0	2	40+0	9 911.008	‡9 911.023	15			9 910.77‡	9 848.0
3	0	1	40−0	9 911.016	9 911.023	7	9 897.277	0.2	9 910.75	9 929.1
3	2	0	21+2	9 996.658					9 992.23‡	
0	2	3	21−2	10 008.533						
4	0	0	31+0	10 188.299	‡10 188.301	2			10 188.86‡	
1	0	3	31−0	10 194.434	10 194.448	15	10 180.702	0.2	10 193.44	
0	0	4	22+0	10 292.758						
1	5	1	20−5	10 742.184						
2	5	0	20+5	10 742.793						
0	5	2	11+5	10 846.547						
2	3	1	30−3	10 904.285						
1	3	2	30+3	10 904.297						
2	1	2	40+1	11 008.713	‡11 008.684	−28				
3	1	1	40−1	11 008.715	11 008.684	−30	10 994.938	0.3	11 007.74	
3	3	0	21+3	11 101.635						
0	3	3	21−3	11 106.729						
4	1	0	40+1	11 294.332						
1	1	3	40−1	11 297.188						
0	1	4	22+1	11 395.406						
1	4	2	30+4	11 990.174						
2	4	1	30−4	11 990.178						
3	2	1	40−2	12 095.230						
2	2	2	40+2	12 095.232						
3	0	2	50+0	12 149.848						
2	0	3	50−0	12 149.852						
0	4	3	21−4	12 193.457						
3	4	0	21+4	12 194.578						
4	2	0	31+2	12 388.432						
1	2	3	31−2	12 389.023						
0	2	4	22+2	12 488.023						
1	0	4	41+0	12 524.564						
4	0	1	41−0	12 525.150						
5	0	0	32+0	12 696.428						
0	0	5	32−0	12 735.256						

*The levels and $P1$ positions are in units of cm^{-1} while the observed − calculated are in units of 10^{-3} cm^{-1}. The observed line intensities are in units of 10^{-5} cm^{-2} atm^{-1} at room temperature; the ν_2 values are from refs. 6 and 7. Some of these intensities may be unreliable indicators of band strengths because the values were obtained from only one or two optical densities and because these lines may be overlapped by other transitions.

†Labeling of the levels differs from that of refs. 3 and 15; our labeling is based on the mixing coefficients originating from the Darling–Dennison resonance interactions between vibrational states and theirs on the contribution of the basis function. The local mode labels follow the scheme of ref. 20.

‡Energy levels for the (040),(400), (050), (202), and (212) states were obtained by fitting rotational levels available with uncertainties of 0.005 cm^{-1}. The (050) state was assigned during the revision of the manuscript and was therefore not included in the vibrational fit.

TABLE 3. Vibrational spectroscopic constants of $H_2{}^{32}S$*

Parameter	Value (cm^{-1})	Parameter	Value (cm^{-1})
ω_1	2719.1770 (760)	$y_{122} \times 100$	−5.82 (190)
ω_2	1212.840 (170)	y_{123}	−1.141 6 (240)
ω_3	2735.8241 (860)	$y_{222} \times 100$	−6.324 (850)
x_{11}	−24.2588 (120)	$y_{233} \times 100$	8.87 (200)
x_{12}	−17.0492 (800)		
x_{13}	−94.9594 (210)	Γ_{DD}	−23.274 98 (790)
x_{22}	−5.3160 (740)	γ_2	0.475 7 (120)
x_{23}	−21.3253 (860)		
x_{33}	−24.4936 (160)		

*Estimated uncertainties in the last digits (in parentheses) are one standard deviation. Number of levels, 30. Number of parameters, 15; rms, cm^{-1}, 0.037. Max. deviation, cm^{-1}, 0.072.

The intensities are given as an indication of relative band strengths. However, a number of caveats apply. The values are determined in normal isotopic abundance, rather than for a 100% $H_2{}^{32}S$ sample. At best (for the 4 μm triad), the accuracies are ±5%. Except for the first triad, these intensities were retrieved from only one or two optical densities, rather than the usual five or six scans; therefore they may have a systematic offset of perhaps ±20% that will require correction after more spectra are recorded. Intensities of lines weaker than 10^{-5} cm^{-2} atm^{-1} are accurate to only ±30%. The reported absorption intensity may contain contributions from other transitions and thus be too high. Finally, even if the measurement is good, caution should be exercised in extrapolating one intensity into a band strength. We note that Lechuga–Fossat et al. [8] required a seven-term dipole moment expansion to fit measured intensities of the first triad; the higher overtones are expected to have many resonances that greatly perturb intensities. Additional intensity measurements are planned, and their analyses will be included in a series of "polyad" articles. Nevertheless, the intensities listed in Table 2 correctly indicate a surprising result seen qualitatively in Fig. 1 and in refs. 8 and 11; in H_2S, the combination bands are relatively strong compared to the fundamentals.

4. The vibrational energy levels of $H_2{}^{32}S$

The observed band origins have been used to determine the effective vibrational Hamiltonian constants and to calculate the highly excited vibrational levels. The effective vibrational Hamiltonian is the "spectroscopic Hamiltonian" of ref. 14 that includes the high anharmonic terms:

$$H = \sum_{ij} H_{ij}|i\rangle\langle j|$$

where

$$H_{ii} = \sum_{\lambda} \omega_\lambda\left(v_\lambda^i + \frac{1}{2}\right) + \sum_{\lambda,\mu\geq\lambda} x_{\lambda,\mu}\left(v_\lambda^i + \frac{1}{2}\right)\left(v_\mu^i + \frac{1}{2}\right) + \sum_{\lambda,\mu\geq\lambda,\nu\geq\mu} y_{\lambda\mu\nu}\left(v_\lambda^i + \frac{1}{2}\right)\left(v_\mu^i + \frac{1}{2}\right)\left(v_\nu^i + \frac{1}{2}\right)\cdots$$

$$H_{ij} = \left\{\Gamma_{DD} + \gamma_1\left(v_1 + \frac{1}{2} \pm 2\right) + \gamma_2\left(v_2 + \frac{1}{2}\right) + \gamma_3\left(v_3 + \frac{1}{2} \mp 2\right)\right\}\left\{\left(v_1 + \frac{1}{2} \pm \frac{1}{2}\right)\left(v_1 + \frac{1}{2} \pm \frac{3}{2}\right)\left(v_3 + \frac{1}{2} \mp \frac{3}{2}\right)\left(v_3 + \frac{1}{2} \mp \frac{1}{2}\right)\right\}^{1/2}$$

if

$$|i\rangle = |v_1\ v_2\ v_3\rangle, \quad |j\rangle = |v_1 \pm 2\ v_2\ v_3 \mp 2\rangle \qquad \text{Darling–Dennison resonance}$$

The spectroscopic parameters determined are the harmonic frequencies ω_1, ω_2, and ω_3, anharmonic x_{ij}, y_{ijk} constants, and the coupling Darling–Dennison resonance constants Γ_{DD} and γ_2. The Fermi resonance was not included in the calculations because it was found to be insignificant. The fitted vibrational parameters of hydrogen sulfide are shown in Table 3 together with estimated uncertainties (one standard deviation). It may be seen that all the fitted constants are generally well determined. However, some of these (ω_2, x_{22}, y_{222}) have correlation coefficients up to 0.9.

Table 2 shows the vibrational energy levels of H_2S up to 13 000 cm^{-1}; the nine columns give the normal and local mode assignments, the fitted and experimental values and the differences, the line positions and intensities of the observed $P1$ lines, and calculated values from refs. 3 and 15. The local modes are ascribed in the manner used by ref. 20. The maximum difference between observed and calculated vibrational energy levels is equal to 0.072 cm^{-1}, and the standard deviation is 0.038 cm^{-1} for 31 observed band centers. Although the fit does not reproduce the band centers to their experimental accuracies, it has to be emphasized that this vibrational energy levels calculation is the best in the literature to date. We believe that reproduction of the experimental data at this level does provide a useful prediction of the highly excited states.

The results of the "ab initio" calculation [15] of the vibrational constants and levels (column 9, Table 2) seem to be in qualitative agreement with our data. We do note that there are some large differences between the experimental values and the ab initio

TABLE 4. The energy differences in cm^{-1} between A1 and B1 stretching pairs

	$n = 1$	$E_{B1} - E_{A1}$	$n = 2$	$E_{B1} - E_{A1}$	$n = 3$	$E_{B1} - E_{A1}$	$n = 4$	$E_{B1} - E_{A1}$
$v = 0$	(100, 001)	14.1	(200, 101)	2.3	(102, 201)	0.2	(202, 301)	0.0
$v = 1$	(110, 011)	10.1	(210, 111)	1.1	(112, 211)	0.0	(212, 311)	0.0
$v = 2$	(120, 021)	6.4	(220, 121)	0.3	(122, 221)	−0.0	(222, 321)	0.0
$v = 3$	(130, 031)	3.0	(230, 131)	−0.3	(132, 231)	−0.0	(232, 331)	0.0
$v = 4$	(140, 041)	−0.1	(240, 141)	−0.5	(142, 241)	−0.0	(242, 341)	0.0
$v = 5$	(150, 051)	−2.9	(250, 151)	−0.6	(152, 251)	0.0	(252, 351)	0.0

*v is the number of bending quanta of ν_2. n is the total number of stretching quanta of ν_1 and ν_3. The stretching pairs are shown in parentheses.

calculations for the (040) state and other higher vibrational states involving the bending vibration. The levels involving low excitation of the bending mode ($\nu_2 < 3$) calculated by Kozin and Jensen [3] using the variational MORBID (Morse Oscillator Rigid Bender Internal Dynamics) method (column 8, Table 2) agree within 1 cm^{-1} with our results. For states involving the excited bending vibration, the differences between our and the Kozin, Jensen calculations range from 2 cm^{-1} for the (040) state to 30 cm^{-1} for the highest bending state (080). Note that in the case of our calculations, the agreement for the (040) state is satisfactory because its observed upper state level was used in our fitting, while in the Kozin, Jensen paper the (040) energy value is purely a prediction.

The MORBID approach uses the exact vibration–rotation Hamiltonian with the intramolecular potential energy function having a reasonable asymptotic behavior. Energy levels are calculated by a "direct" numerical diagonalization, and the potential energy function parameters are fitted to a large number of rotational–vibrational levels of four isotopic species of hydrogen sulfide. The MORBID calculations tend to give accurate energy levels; hence the good agreement between our levels and those predicted within the MORBID approach is evidence of the validity of the effective vibrational Hamiltonian method.

5. The local modes in hydrogen sulfide

5.1. *Vibrational energy spectrum of H_2S and local mode limit*

The traditional theory of vibrational–rotational spectra is based on the concept of normal coordinates and a perturbation treatment of vibration–rotation interactions with anharmonic corrections and relevant effective rotational Hamiltonians [16]. The conventional approach has been successful in explaining the spectra caused by transitions to low-lying vibrational states, but other approaches are required for highly excited vibrational states. The local mode model has been successfully applied to fit the vibrational spectra of H_2X, XH_3, XH_4, and several other types of molecules (see, for instance, refs. 17–28). In this treatment, the molecule is represented as the sum of independent Morse oscillators with a weak potential and kinetic couplings between them while the bending vibration is frozen. The local mode model does explain the spacing between states of symmetric and asymmetric vibrational mode (the local mode pair) and the degeneracy of these levels under high excitation.

An extensive set of H_2S vibrational–rotation energies (experimental and calculated) gives us a unique opportunity to understand the local mode limit in some detail. We first note that the relation predicted by Lehmann [26] and described by Mills and Robiette [27] is satisfied by the fitted H_2S parameters shown in Table 3.

$$x_{11} = x_{33} = 0.25x_{13} = \Gamma_{DD}$$

or

$$-24.3 \approx -24.5 \approx -23.7 \approx -23.3$$

Secondly, we can determine the energy where the "local mode limit" is reached so that the stretching modes become degenerate. The energy differences between stretching pairs ($E_{B1} - E_{A1}$) are presented in Table 4. These clearly demonstrate the influence of the bending vibration on the stretching pair spacing. When bending vibration is frozen (column 1 in the Table 4) the stretching pairs become degenerate beginning at $n = 3$. When the number of the stretching quanta are small, the increase of the bending vibration quanta leads to a sharp decrease of $E_{B1} - E_{A1}$. When the number of the stretching quanta exceeds two, the bending vibration does not affect the degeneracy of the pairs.

5.2. *Rotational energy levels at the local mode limit*

Despite extensive studies of local mode vibrational motion in different types of molecules and the theoretical analysis of rotational structure of an isolated mode doublet, there is only limited information about the rotation–vibration energy structure for the case of local mode behavior (see ref. 25). Existing models employ simplifying assumptions about the intramolecular potential energy function [23]. Little has been reported about the rotational structure in the local mode limit.

In the present study, we examined the rotation–vibration energy levels of the nearly degenerate pairs of vibrational states corresponding to the excitation of three and four quanta of the stretching vibration. Band origins and rotational constants were determined by fitting experimental energy levels. For example, the calculated and observed upper state levels, the differences between observed and calculated values, and the mixing coefficients for the {(301)–(202)} and {(311)–(212)} local mode pairs are presented in Tables 5 and 6, respectively. We noted some interesting features. First, all levels of the stretching pairs are at least doubly degenerate, despite the fact that they are determined from different sets of lines of parallel and perpendicular bands. In the first pair, the degenerate pairs consist of one level belonging to (301) and another one belonging to

TABLE 5. Upper state energy levels (in cm^{-1}) and mixing coefficients for the (301) and (202) vibrational states of $H_2{}^{32}S$

			(301)					(202)				
J	K_a	K_c	E_{calcd}	E_{obsd}	O–C	Mixing		E_{calcd}	E_{obsd}	O–C	Mixing	
0	0	0	9 911.022	9 911.022	0	100.0	0.0	9 911.022			0.0	100.0
1	0	1	9 923.854	9 923.856	2	83.0	17.0	9 923.854	9 923.849	−4	17.0	83.0
1	1	1	9 925.371	9 925.369	−1	83.0	17.0	9 925.371			17.0	83.0
1	1	0	9 929.250	9 929.253	2	100.0	0.0	9 929.250			0.0	100.0
2	0	2	9 947.148	9 947.143	−5	54.4	45.6	9 947.148	9 947.141	−7	45.5	54.5
2	1	2	9 946.784	9 946.777	−6	53.4	46.6	9 946.784	9 946.781	−2	46.7	53.3
2	1	1	9 958.779	9 958.782	2	82.9	17.1	9 958.779	9 958.772	−6	17.1	82.9
2	2	1	9 963.323	9 963.322	0	82.9	17.1	9 963.323	9 963.315	−7	17.1	82.9
2	2	0	9 966.046	9 966.047	0	98.9	1.1	9 966.046			1.1	98.9
3	0	3	9 978.421	9 978.421	0	86.6	13.4	9 978.422			13.0	87.0
3	1	3	9 978.364	9 978.362	−1	86.8	13.2	9 978.364			13.6	86.4
3	1	2	10 001.776	10 001.772	−3	54.8	45.2	10 001.776	10 001.774	−1	45.1	54.9
3	2	2	10 000.081	10 000.079	−1	50.4	49.6	10 000.081	10 000.087	5	49.6	50.4
3	2	1	10 011.375	10 011.381	5	82.2	17.8	10 011.375	10 011.370	−4	17.8	82.2
3	3	1	10 020.387	10 020.386	0	82.5	17.5	10 020.387			17.6	82.4
3	3	0	10 021.965	10 021.960	−4	95.6	4.4	10 021.965	10 021.958	−6	4.4	95.6
4	0	4	10 018.757	10 018.758	0	99.4	0.6	10 018.757	10 018.752	−4	0.6	99.4
4	1	4	10 018.749	10 018.752	2	99.3	0.7	10 018.749	10 018.758	8	0.7	99.3
4	1	3	10 050.634	10 050.634	0	85.7	14.3	10 050.633	10 050.616	−16	14.3	85.7
4	2	3	10 050.252	10 050.251	0	84.2	15.8	10 050.252	10 050.245	−6	15.8	84.2
4	2	2	10 074.782	10 074.780	−1	55.5	44.5	10 074.782			44.5	55.5
4	3	2	10 070.300	10 070.290	−9	45.9	54.1	10 070.300	10 070.301	0	54.1	45.9
4	3	1	10 081.962	10 081.965	2	79.8	20.2	10 081.962			20.2	79.8
4	4	1	10 096.656	10 096.655	0	81.3	18.7	10 096.656	10 096.647	−8	18.7	81.3
4	4	0	10 097.433	10 097.432	0	90.4	9.6	10 097.433	10 097.423	−9	9.6	90.4
5	0	5	10 068.042	10 068.039	−2	60.2	39.8	10 068.041	10 068.040	0	46.9	53.1
5	1	5	10 068.041	10 068.040	0	53.1	46.9	10 068.042	10 068.039	−2	39.8	60.2
5	1	4	10 108.901	10 108.907	5	98.5	1.5	10 108.901			1.5	98.5
5	2	4	10 108.837	10 108.835	−1	98.3	1.7	10 108.836			1.7	98.3
5	2	3	10 140.678	10 140.672	−5	84.5	15.5	10 140.678	10 140.676	−1	15.5	84.5
5	3	3	10 139.267	10 139.266	0	79.5	20.5	10 139.266			20.6	79.4
5	3	2	10 166.294	10 166.291	−2	56.7	43.3	10 166.294	10 166.294	0	43.3	56.7
5	4	2	10 157.450	10 157.444	−5	42.0	58.0	10 157.451			58.0	42.0
5	4	1	10 171.040	10 171.036	−3	74.4	25.6	10 171.040	10 171.036	−3	25.6	74.4
5	5	1	10 192.177	10 192.177	0	79.4	20.6	10 192.177			20.6	79.4
5	5	0	10 192.518	10 192.519	0	85.0	15.0	10 192.517	10 192.512	−4	15.0	85.0
6	0	6	10 126.252	10 126.250	−1	99.1	0.9	10 126.252	10 126.250	−1	47.6	52.4
6	1	6	10 126.252	10 126.250	−1	52.4	47.6	10 126.253	10 126.250	−2	0.9	99.1
6	1	5	10 176.181	10 176.187	5	94.4	5.6	10 176.182	10 176.176	−5	4.4	95.6
6	2	5	10 176.171	10 176.176	4	95.6	4.4	10 176.172	10 176.187	14	5.6	94.4
6	2	4	10 216.616	10 216.620	3	96.8	3.2	10 216.616			3.2	96.8
6	3	4	10 216.306	10 216.307	0	95.8	4.2	10 216.306			4.2	95.8
6	3	3	10 248.563	10 248.568	4	82.8	17.2	10 248.563			17.2	82.8
6	4	3	10 244.849			71.5	28.5	10 244.850	10 244.833	16	28.5	71.5
6	4	2	10 261.842	10 261.837	−4	60.1	39.9	10 261.843			39.9	60.1
6	5	2	10 276.432			41.3	58.7	10 276.432	10 276.432	0	58.7	41.3
6	5	1	10 279.171	10 279.176	4	65.7	34.3	10 279.171			34.3	65.7
6	6	1	10 306.924	10 306.926	1	77.0	23.0	10 306.924	10 306.920	−3	3.0	77.0
6	6	0	10 307.063	10 307.065	2	80.2	19.8	10 307.062	10 307.077	15	19.8	80.2
7	0	7	10 193.376	10 193.377	0	98.9	1.1	10 193.376	10 193.375	0	49.0	51.0
7	1	7	10 193.376	10 193.375	0	51.0	49.0	10 193.377	10 193.377	0	1.1	98.9
7	1	6	10 252.368	10252.363	−4	89.1	10.9	10 252.369	10 252.363	−5	5.2	94.8
7	2	6	10 252.367	10 252.363	−3	94.8	5.2	10 252.367	10 252.363	−3	10.9	89.1
7	2	5	10 301.762	10 301.758	−3	94.1	5.9	10 301.762			5.5	94.5
7	3	5	10 301.703	10 301.720	16	94.4	5.6	10 301.703	10 301.710	6	6.0	94.0
7	3	4	10 341.752	10 341.764	11	94.0	6.0	10 341.751			6.0	94.0
7	4	4	10 340.693	10 340.696	2	90.8	9.2	10 340.693			9.2	90.8
7	4	3	10 374.354			80.8	19.2	10 374.354			19.2	80.8
7	5	3	10 366.698	10 366.692	−5	62.2	37.8	10 366.697			37.8	62.2
7	5	2	10 405.282			61.3	38.7	10 405.282	10 405.297	14	38.7	61.3
7	6	2	10 383.948	10 383.953	4	40.5	59.5	10 383.948			59.5	40.5
7	6	1	10 406.679			55.4	44.6	10 406.678			44.6	55.4
7	7	1	10 440.815	10 440.809	−6	74.2	25.8	10 440.815	10 440.808	−7	25.8	74.2
7	7	0	10 440.868	10 440.866	−1	76.0	24.0	10 440.868	10 440.865	−2	24.0	76.0
8	0	8	10 269.402	10 269.398	−3	99.7	0.3	10 269.402	10 269.398	−3	49.5	50.5
8	1	8	10 269.402	10 269.405	2	50.5	49.5	10 269.403	10 269.405	1	0.3	99.7
8	1	7	10 337.440	10 337.445	4	99.1	0.9	10 337.440	10 337.445	4	1.3	98.7
8	2	7	10 337.439	10 337.439	0	98.7	1.3	10 337.438	10 337.439	0	0.9	99.1
8	2	6	10 395.818			86.6	13.4	10 395.818			13.1	86.9

TABLE 5. (*concluded*)

			(301)					(202)				
J	K_a	K_c	E_{calcd}	E_{obsd}	O–C	Mixing		E_{calcd}	E_{obsd}	O–C	Mixing	
8	3	6	10 395.808	10 395.794	−13	86.8	13.2	10 395.808	10 395.808	0	13.4	86.6
8	3	5	10 444.553			91.9	8.1	10 444.552			8.2	91.8
8	4	5	10 444.312			91.4	8.6	10 444.313			8.6	91.4
8	4	4	10 484.219	10 484.200	−18	90.1	9.9	10 484.217			9.9	90.1
8	5	4	10 481.399			82.6	17.4	10 481.399			17.4	82.6
8	5	3	10 504.923	10 504.929	5	46.0	54.0	10 504.924			54.0	46.0
8	6	3	10 553.512			53.9	46.1	10 553.512			46.1	53.9
8	6	2	10 552.867			64.5	35.5	10 552.867			35.5	64.5
8	7	2	10 524.359			44.1	55.9	10 524.360			55.9	44.1
8	7	1	10 518.150	10 518.160	9	78.7	21.3	10 518.149			21.3	78.7
8	8	1	10 593.728			71.2	28.8	10 593.728			28.8	71.2
8	8	0	10 593.746	10 593.745	0	72.2	27.8	10 593.747			27.8	72.2
9	0	9	10 354.317	10 354.316	0	55.3	44.7	10 354.317	10 354.321	3	44.3	55.7
9	1	9	10 354.317	10 354.316	0	55.7	44.3	10 354.317	10 354.321	3	44.7	55.3
9	1	8	10 431.377	10 431.385	7	98.9	1.1	10 431.377	10 431.385	7	46.3	53.7
9	2	8	10 431.377	10 431.372	−4	53.7	46.3	10 431.375	10 431.372	−2	1.1	98.9
9	2	7	10 498.712			81.1	18.9	10 498.711			28.4	71.6
9	3	7	10 498.708	10 498.708	0	71.6	28.4	10 498.709			18.9	81.1
9	3	6	10 556.341			83.2	16.8	10 556.341			17.4	82.6
9	4	6	10 556.290			82.6	17.4	10 556.291			16.9	83.1
9	4	5	10 604.340			88.4	11.6	10 604.341			11.6	88.4
9	5	5	10 603.557			87.0	13.0	10 603.558			13.0	87.0
9	5	4	10 644.004			85.3	14.7	10 644.005			14.7	85.3
9	6	4	10 637.862			71.8	28.2	10 637.864			28.2	71.8
9	6	3	10 659.950			51.8	48.2	10 659.949			48.2	51.8
9	7	3	10 719.412			61.4	38.6	10 719.412			38.6	61.4
9	7	2	10 719.135			67.7	32.3	10 719.134			32.3	67.7
9	8	2	10 683.614			49.9	50.1	10 683.615			50.1	49.9
9	8	1	10 680.044			76.4	23.6	10 680.045			23.6	76.4
9	9	1	10 765.521			68.2	31.8	10 765.521			31.8	68.2
9	9	0	10 765.526			68.7	31.3	10 765.527			31.3	68.7

*O–C = observed − calculated band centers in units of 10^{-3} cm^{-1}.

(202). The degeneracy is within 0.018 cm^{-1} for levels listed in Table 5.

To model the observed levels, the effective rotational Hamiltonian is written in the usual manner; apart from the Watson-type "diagonal" Hamiltonian, it contains the Coriolis-type "resonance" operator. If we use the Hamiltonian with different rotational and centrifugal distortion constants for the two vibrational states belonging to the given local mode pair, we find that the parameters of the two states are very similar. For instance, the rotational constants of the (301) and (202) pair are 9.615 98 ± 0.000 60, 8.614 83 ± 0.000 71, 4.476 45 ± 0.000 13 and 9.615 89 ± 0.000 69, 8.613 15 ± 0.000 77, 4.476 77 ± 0.000 17 for the A, B, and C constants, respectively, and the centrifugal distortion constants are equally close. If we force the rotational constants of the pairs to be equal, reducing the number of fitted parameters from 17 to 9, the quality of the fitting does not change very much; in the first case, the standard deviation is 0.005 cm^{-1} and for the second it is 0.006 cm^{-1}. Thus, one can conclude that the highly excited local mode vibrations lead to an alignment of rotational and centrifugal distortion constants for the paired states and that the parameters become identical. As a consequence one can use for the calculations the simple models with fewer adjusted parameters. The fitted parameters for these states are presented in Table 7. The Hamiltonian reproduces the experimental data well enough to assign unambiguously the spectrum recorded at 0.02 cm^{-1} resolution. For 120 energy levels of (301)–(202) and 129 levels of (311)–(212), the standard deviations are 0.006 cm^{-1}, and the largest deviation is 0.017 cm^{-1}.

As seen from Tables 5 and 6, the mixing between rotational sublevels is strong. There are numerous levels with approximately fifty–fifty mixing, and the maximum of the mixing shifts toward the larger values of the K_a quantum number with increasing J. This causes the strengthening of the weak component of local mode pair (e.g., (202)). As a consequence, there are a large number of lines that are actually doublets. This leads to some difficulties in the energy levels determination. We also found examples of fourfold clustering in the (301)–(202) pair starting with $J = 4$ levels at $K_a = 0$ and 1 of both states. For $J = 6$, the degeneracy is 0.001 cm^{-1}, and analogous clustering takes place for $K_a = 1$ and 2 levels starting at $J = 6$, and for $K_a = 2$ and 3 at $J = 8$ etc. This kind of fourfold clustering was previously predicted by Lehmann [23] and later confirmed by Kozin and Jensen during MORBID calculations for the ν_1/ν_3 bands of H_2S [3] and H_2Se [28]. This type of clustering is formed by "coexistence" of two energy doublets belonging to the states of a local mode pair. The present result is experimental evidence of this phenomena at low J and K_a values.

6. Conclusion

The large set of rotational–vibration energy levels obtained from the high-resolution Fourier transform spectra of H_2S up to 11 147 cm^{-1} has permitted detailed studies of its vibrational structure in the local mode limit. The high excited bending vibrational states (030), (040), (050), (130), and (031) have been analyzed for the first time so that the bending–vibrational interactions could be investigated. The local mode limit is clearly

TABLE 6. Upper state energy levels (in cm^{-1}) and mixing coefficient for the (311) and (212) vibrational states of $H_2{}^{32}S$

			(311)					(212)				
J	K_a	K_c	E_{calcd}	E_{obsd}	O−C	Mixing		E_{calcd}	E_{obsd}	O−C	Mixing	
0	0	0	11 008.684	11 008.684	0	100.0	0.0	11 008.684			0.0	100.0
1	0	1	11 021.667	11 021.669	1	83.3	16.7	11 021.667	11 021.670	2	16.7	83.3
1	1	1	11 023.299	11 023.301	1	83.3	16.7	11 023.299			16.7	83.3
1	1	0	11 027.451	11 027.451	0	100.0	0.0	11 027.451	11 027.459	7	0.0	100.0
2	0	2	11 045.107	11 045.107	0	54.0	46.0	11 045.107	11 045.115	7	46.1	53.9
2	1	2	11 044.714	11 044.711	−2	52.8	47.2	11 044.713	11 044.716	2	47.1	52.9
2	1	1	11 057.555	11 057.555	0	83.3	16.7	11 057.555			16.7	83.3
2	2	1	11 062.443	11 062.441	−1	83.3	16.7	11 062.443	11 062.440	−2	16.7	83.3
2	2	0	11 065.352	11 065.355	3	98.9	1.1	11 065.352			1.1	98.9
3	0	3	11 076.331	11 076.336	4	86.3	13.7	11 076.331	11 076.335	3	13.9	86.1
3	1	3	11 076.270	11 076.272	2	85.9	14.1	11 076.270	11 076.270	0	13.9	86.1
3	1	2	11 099.519	11 099.518	0	50.1	49.9	11 099.519	11 099.517	−1	49.9	50.1
3	2	2	11 101.350	11 101.349	0	45.7	54.3	11 101.351	11 101.356	5	54.3	45.7
3	2	1	11 111.607	11 111.604	−3	82.5	17.5	11 111.607	11 111.604	−3	17.5	82.5
3	3	1	11 121.299	11 121.299	0	82.8	17.2	11 121.299	11 121.299	0	17.2	82.8
3	3	0	11 122.979	11 122.980	0	95.6	4.4	11 122.979	11 122.979	0	4.4	95.6
4	0	4	11 116.508	11 116.510	1	99.5	0.5	11 116.508	11 116.506	−1	0.5	99.5
4	1	4	11 116.500	11 116.506	5	99.5	0.5	11 116.500	11 116.510	9	0.5	99.5
4	1	3	11 150.649	11 150.651	1	85.8	14.2	11 150.649	11 150.641	−8	14.2	85.8
4	2	3	11 150.235	11 150.232	−2	84.3	15.7	11 150.234	11 150.237	2	15.7	84.3
4	2	2	11 176.514	11 176.511	−2	55.0	45.0	11 176.514			45.0	55.0
4	3	2	11 171.673	11 171.665	−7	45.5	54.5	11 171.674	11 171.672	−1	54.5	45.5
4	3	1	11 184.167	11 184.165	−1	80.1	19.9	11 184.167	11 184.166	0	19.9	80.1
4	4	1	11 199.956	11 199.957	0	81.6	18.4	11 199.956	11 199.955	0	18.4	81.6
4	4	0	11 200.779	11 200.778	0	90.5	9.5	11 200.779	11 200.783	3	9.5	90.5
5	0	5	11 165.518	11 165.524	6	96.7	3.3	11 165.518	11 165.523	5	0.9	99.1
5	1	5	11 165.516	11 165.524	8	99.1	0.9	11 165.517	11 165.524	7	3.3	96.7
5	1	4	11 209.280	11 209.286	5	98.7	1.3	11 209.281			1.3	98.7
5	2	4	11 209.211	11 209.210	0	98.5	1.5	11 209.211			1.5	98.5
5	2	3	11 243.293	11 243.297	3	84.6	15.4	11 243.294	11 243.293	0	15.4	84.6
5	3	3	11 241.761	11 241.756	−4	79.5	20.5	11 241.761	11 241.753	−7	20.5	79.5
5	3	2	11 270.725	11 270.732	7	56.3	43.7	11 270.726	11 270.721	−4	43.7	56.3
5	4	2	11 261.189	11 261.181	−8	41.7	58.3	11 261.190			58.3	41.7
5	4	1	11 275.769	11 275.775	6	74.7	25.3	11 275.767	11 275.765	−1	25.3	74.7
5	5	1	11 298.449	11 298.449	0	79.8	20.2	11 298.449	11 298.449	0	20.2	79.8
5	5	0	11 298.809	11 298.811	1	85.2	14.8	11 298.809	11 298.809	0	14.8	85.2
6	0	6	11 223.335	11 223.333	−1	99.0	1.0	11 223.335	11 223.333	−1	0.7	99.3
6	1	6	11 223.336	11 223.333	−2	99.3	0.7	11 223.336	11 223.333	−2	1.0	99.0
6	1	5	11 276.820	11 276.817	−2	91.7	8.3	11 276.821	11 276.819	−1	4.9	95.1
6	2	5	11 276.810	11 276.819	9	95.1	4.9	11 276.811	11 276.817	6	8.3	91.7
6	2	4	11 320.090	11 320.100	9	97.0	3.0	11 320.091			3.0	97.0
6	3	4	11 319.755	11 319.744	10	96.0	4.0	11 319.755	11 319.744	−10	4.0	96.0
6	3	3	11 354.265	11 354.269	3	83.0	17.0	11 354.265	11 354.262	−2	17.0	83.0
6	4	3	11 350.244	11 350.243	0	71.6	28.4	11 350.243	11 350.247	3	28.4	71.6
6	4	2	11 384.109	11 384.114	4	58.3	41.7	11 384.108			41.7	58.3
6	5	2	11 368.395	11 368.402	7	39.7	60.3	11 368.396	11 368.403	7	60.3	39.7
6	5	1	11 387.005	11 387.009	3	65.9	34.1	11 387.004			34.1	65.9
6	6	1	11 416.738			77.4	22.6	11 416.738	11 416.738	0	22.6	77.4
6	6	0	11 416.885	11 416.881	−3	80.5	19.5	11 416.884			19.5	80.5
7	0	7	11 289.949	11 289.949	0	54.4	45.6	11 289.948	11 289.949	0	0.5	99.5
7	1	7	11 289.949	11 289.949	0	99.5	0.5	11 289.949	11 289.949	0	45.6	54.4
7	1	6	11 353.158	11 353.152	−5	61.7	38.3	11 353.157	11 353.152	−4	15.5	84.5
7	2	6	11 353.156	11 353.152	−3	84.5	15.5	11 353.156	11 353.152	−3	38.3	61.7
7	2	5	11 406.014			92.3	7.7	11 406.014			7.3	92.7
7	3	5	11 405.951	11 405.958	6	92.6	7.4	11 405.952			7.8	92.2
7	3	4	11 448.766			94.2	5.8	11 448.765			5.8	94.2
7	4	4	11 447.621	11 447.610	−10	91.1	8.9	11 447.621			8.9	91.1
7	4	3	11 483.626			81.2	18.8	11 483.626			18.8	81.2
7	5	3	11 475.351			62.4	37.6	11 475.349			37.6	62.4
7	5	2	11 516.747			60.9	39.1	11 516.748			39.1	60.9
7	6	2	11 493.798			40.4	59.6	11 493.798			59.6	40.4
7	6	1	11 518.215			55.8	44.2	11 518.213			44.3	55.7
7	7	1	11 554.719	11 554.720	0	74.6	25.4	11 554.718			25.4	74.6
7	7	0	11 554.772			76.3	23.7	11 554.773	11 554.786	12	23.7	76.3
8	0	8	11 365.350	11 365.350	0	99.7	0.3	11 365.351	11 365.350	0	0.3	99.7
8	1	8	11 365.349	11 365.350	0	99.7	0.3	11 365.349	11 365.350	0	0.3	99.7
8	1	7	11 438.269	11 438.263	−5	98.8	1.2	11 438.268	11 438.263	−4	45.2	54.8
8	2	7	11 438.268	11 438.263	−4	54.8	45.2	11 438.268	11 438.263	−4	1.2	98.8
8	2	6	11 500.747			81.1	18.9	11 500.747			15.2	84.8

TABLE 6. (*concluded*)

J	K_a	K_c	(311) E_{calcd}	E_{obsd}	O–C	Mixing		(212) E_{calcd}	E_{obsd}	O–C	Mixing	
8	3	6	11 500.735	11 500.728	−7	84.8	15.2	11 500.736	11 500.728	−8	18.9	81.1
8	3	5	11 552.837			90.3	9.7	11 552.838			9.7	90.3
8	4	5	11 552.584			89.9	10.1	11 552.584			10.1	89.9
8	4	4	11 595.198			90.4	9.6	11 595.197			9.6	90.4
8	5	4	11 592.157			82.9	17.1	11 592.157			17.1	82.9
8	5	3	11 617.204			45.7	54.3	11 617.203			54.3	45.7
8	6	3	11 669.334			53.5	46.5	11 669.333			46.5	53.5
8	6	2	11 668.659			64.0	36.0	11 668.660			36.0	64.0
8	7	2	11 638.025			44.1	55.9	11 638.026			55.9	44.1
8	7	1	11 631.477			79.1	20.9	11 631.478			20.9	79.1
8	8	1	11 712.238			71.7	28.3	11 712.238			28.3	71.7
8	8	0	11 712.259			72.6	27.4	11 712.259			27.4	72.6

TABLE 7. Fitted constants (in cm^{-1}) of local mode pairs of H_2S

	(301) and (202)	(311) and (212)
E_v	9911.022 5	11008.683 6
A	9.614 81 (29)	9.929 16 (51)
B	8.615 33 (33)	8.841 91 (19)
C	4.476 61 (12)	4.415 53 (61)
$\Delta_k \times 10^3$	3.990 (16)	4.067 (34)
$\Delta_{jk} \times 10^3$	−2.563 (10)	−2.368 2 (44)
$\Delta_j \times 10^4$	6.531 (12)	6.560 9 (51)
$\delta_k \times 10^4$	−3.155 (67)	−6.0
$\delta_j \times 10^4$	2.950 (10)	2.970 5 (29)
$H_k \times 10^6$	1.8	2.83 (53)
C_{xz}	0.569 651 (88)	−0.608 171 (87)
Standard deviation	0.006 cm^{-1}	0.005
Number of levels	120	129

NOTE: Estimated uncertaintes are 1 σ in the last digit. Parameters without uncertainties were held fixed.

demonstrated in several highly excited vibrational states: (211)–(112), (301)–(202), and (311)–(212). The rotational structure of the stretching pairs is completely degenerate from $J = 0$ up to $J = 10$, and the spacing between corresponding levels in the stretching pairs is less than 0.02 cm^{-1}. This allows the mixing of the spectroscopic parameters of one vibrational component with another component of the stretching pair. As a result, a fourfold degeneracy of the $K_a = 0$ and $K_a = 1$ arises at low J values when strong excitation of the local modes occurs. Refinement of the rotational constants and analyses of dipole moment parameters are currently in progress and will be reported later. Database predictions based on ref. 8 and the present results are available for the 4 μm region.

Acknowledgements

The authors thank the Kitt Peak National Observatory/National Solar Observatory for the use of the FTS and C. Plymate and J. Wagner for assistance in obtaining the H_2S spectra. We also thank I. Kozin and P. Jensen for making results available to us prior to publication and K. Lehmann for his detailed review of the manuscript. Part of the research reported in this paper was performed at the Jet Propulsion Laboratory, California Institute of Technology, under contract with the National Aeronautics and Space Administration.

1. S. Miller, J. Tennyson, P. Rosmus, J. Senekowitsch, and I.M. Mills. J. Mol. Spectrosc. **143**, 61 (1990).
2. J. Makarevicz and J. Pyka. Mol. Phys. **68**, 107 (1989).
3. I.N. Kozin and P. Jensen. J. Mol. Spectrosc. **163**, 483 (1994).
4. J.-M. Flaud, C. Camy-Peyret, and J.W.C. Johns. Can. J. Phys. **61**, 1462 (1983).
5. C. Camy-Peyret, J.-M. Flaud, L. Lechuga-Fossat, and J.W.C. Johns. J. Mol. Spectrosc. **109**, 300 (1985).
6. L.L. Strow. J. Mol. Spectrosc. **97**, 9 (1983).
7. W.C. Lane, T.H. Edwards, J.R. Gillis, F.S. Bonomo, and F.J. Murcray. J. Mol. Spectrosc. **111**, 320 (1985).
8. L. Lechuga-Fossat, J.-M. Flaud, C. Camy-Peyret, and J.W.C. Johns. Can. J. Phys. **62**, 1889 (1984).
9. L.E. Snyder and T.H. Edwards. J. Mol. Spectrosc. **31**, 347 (1969).
10. O.V. Zotov, V.S. Makarov, O.V. Naumenko, and A.D. Bykov. Atmos. Opt. **4**, 798 (1991).
11. L. Lechuga-Fossat, J.-M. Flaud, C. Camy-Peyret, P. Arcas, and M. Cuisenier. Mol. Phys. **61**, 233 (1987).
12. C.R. Pollock, F.R. Petersen, D.A. Jennings, J.S. Wells, and A.G. Maki. J. Mol. Spectrosc. **99**, 357 (1983).
13. P. Ormsby, B. Winnewisser, M. Winnewisser, K. Narahari Rao, A. Bykov, O. Naumenko, and L. Sinitsa. J. Mol. Spectrosc. In press.
14. B.T. Darling and D.M. Dennison. Phys. Rev. **57**, 128 (1940).
15. J. Senekowitsch, S. Carter, A. Zilch, H.J. Werner, and N.C. Handy. J. Chem. Phys. **90**, 783 (1989).

16. D. Papousek and M.R. Aliev. Molecular vibrational–rotational spectra. Elsevier, Amsterdam. 1982.
17. M.S. Child and L. Halonen. Adv. Chem. Phys. **57**, 1 (1984).
18. L. Halonen. J. Mol. Spectrosc. **120**, 175 (1986).
19. L. Halonen and M.S. Child. Comput. Phys. Commun. **51**, 173 (1988).
20. L. Halonen and T. Carrington, Jr. J. Chem. Phys. **88**, 4171 (1988).
21. M. Halonen, L. Halonen, H. Burger, and P. Moritz. J. Chem. Phys. **95**, 7099 (1991).
22. M. Halonen, L. Halonen, H. Burger, and P. Moritz. Chem. Phys. Lett. **203**, 157 (1993).
23. L. Halonen and A.G. Robiette. J. Chem. Phys. **84**, 6861 (1986).
24. K.K. Lehmann. J. Chem. Phys. **95**, 2361 (1991).
25. H. Burger and G. Graner. J. Mol. Spectrosc. **149**, 491 (1991).
26. K.K. Lehmann. J. Chem. Phys. **79**, 1098 (1983).
27. I.M. Mills and A.G. Robiette. Mol. Phys. **56**, 743 (1985).
28. I.N. Kozin and P. Jensen. J. Mol. Spectrosc. **161**, 186 (1993)